Journal of Microscopy, Vol. 189, Pt 2, February 1998, pp. 114–117.
Received 30 September 1997; accepted 31 October 1997

SHORT COMMUNICATION

A light efficient optically sectioning microscope

M. A. A. NEIL, T. WILSON & R. JUŠKAITIS
Department of Engineering Science, University of Oxford, Parks Road, Oxford OX1 3PJ, U.K.

Key words. Confocal microscopy, optical sectioning.

Summary

We describe a simple method by which optically sectioned images may be obtained. The system geometry is similar to that of a tandem scanning microscope but a one-dimensional grid pattern is used rather than an array of pinholes. This produces a composite image consisting of an optically sectioned image superimposed on a conventional image. A blank sector on the disc is used to provide a wide-field image. Image subtraction yields the optically sectioned image in real time.

The optical sectioning property of the confocal microscope arises from the use of a physical obstruction which prevents light originating in out-of-focus planes from reaching the photodetector (Wilson & Sheppard, 1984; Wilson, 1990). In most single point systems a pinhole or slit aperture is used as the obstruction. These instruments require laser illumination and the confocal image is not usually acquired in real time. Real-time confocal images may be obtained in the tandem scanning microscope (Egger & Petráň, 1967; Xiao *et al.*, 1988) without the need to use laser illumination. These instruments consist of many parallel confocal systems each probing a specific point on the object. The pinhole arrays which form these systems are often arranged in Archimedean spirals on a disc. Since it is necessary that the parallel confocal systems do not interact, the pinholes must be spaced far apart. This has two important consequences. The first is that the specimen is sparsely probed and hence the disc must be rotated so as to image the entire specimen. The second consequence of the need to use widely spaced pinholes is that only a small amount—typically of the order of 1%—of the light available for imaging is used. In an attempt to improve the light budget of the real-time confocal microscope, alternative approaches based on aperture correlation techniques have been proposed (Juškaitis *et al.*, 1996; Wilson *et al.*, 1996). The light budget of these instruments may be as high as 50% depending on the implementation.

The instruments and development we have described above have all been aimed at producing real-time confocal images using standard microscope illumination systems. In the following we shall relax the requirement that the image formation should be formally equivalent to that of the confocal microscope but merely that it should exhibit optical sectioning. We retain the geometry of the tandem scanning or direct view microscope but introduce an arbitrary intensity transmittance, $S(t)$, for the disc. In order to characterize optical sectioning we consider the image signal from a plane mirror specimen as the microscope is defocused. We follow Wilson & Hewlett (1991) and write this axial response as

$$I(u) = \int Q(t)|h(2u, t)|^2 \mathrm{d}t \tag{1}$$

where $Q(t) = S(t) \otimes S(-t)$, the symbol $\otimes$ denotes the convolution operation and h is the amplitude point spread function. We have elected to work in lateral (t) and axial (u) optical coordinates which are related to real lateral distance (x) and real defocus (z) by

$$t = \frac{2\pi}{\lambda} x\, n \sin\alpha \tag{2}$$

and

$$u = \frac{8\pi}{\lambda} n\, z \sin^2 \frac{\alpha}{2} \tag{3}$$

where $n \sin\alpha$ denotes the numerical aperture and λ the wavelength.

We now assume that the mask intensity transmittance is periodic such that $Q(t)$ may be written as a Fourier cosine series

$$Q(t) = \sum_{l=-0}^{\infty} c_l \cos(l\tilde{\nu}t) \tag{4}$$

where $\tilde{\nu}$ is the normalized spatial frequency which is related to the actual spatial frequency via $\tilde{\nu} = \nu\lambda/n \sin\alpha$.

If we substitute Eq. (4) into Eq. (1) and recall that the amplitude point spread function, h, is given by the Fourier

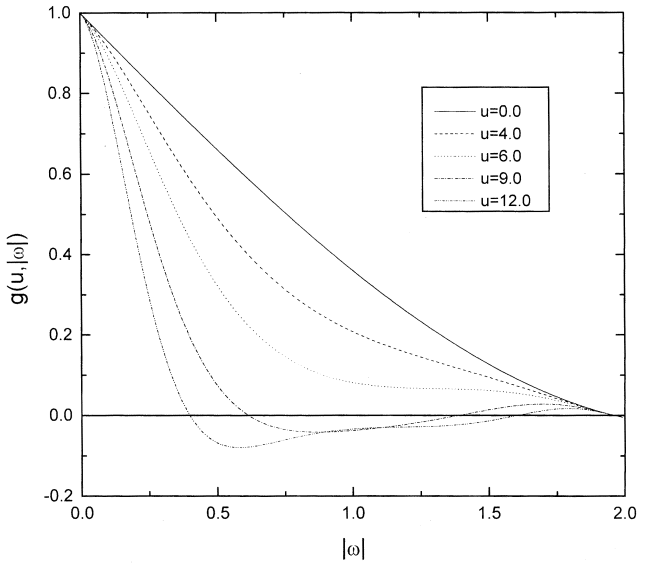

Fig. 1. The form of the function $g(u, |\omega|)$ as a function of $|\omega|$ for a variety of values of u.

transform of the pupil function, P, then

$$I(u) = \sum_{l=-\infty}^{\infty} c_l g(2u, l\tilde{\nu}) \tag{5}$$

where $g(u, |\omega|) = P \otimes P^*(u, |\omega|)$ and is cut-off for $|\omega| \geqslant 2$. It is a straightforward matter to evaluate $g(u, |\omega|)$ directly but an approximation due to Stockseth (1969) will suffice for our purposes. This gives

$$g(u, |\omega|) = f(|\omega|)\left\{2\frac{J_1(us)}{us}\right\} \tag{6}$$

where $f(|\omega|) = 1 - 0{\cdot}69|\omega| + 0{\cdot}0076|\omega|^2 + 0{\cdot}043|\omega|^3$, $s = |\omega|(1 - |\omega|/2)$ and $J_1(\cdot)$ denotes the first-order Bessel function of the first kind. We plot $g(u, |\omega|)$ in Fig. 1 and we see that the function decays with defocus for all values of $|\omega|$ except $|\omega| = 0$. This permits us to rewrite Eq. (5) as

$$I(u) = c_0 + \sum_{l=1}^{\infty} c_l g(2u, l\tilde{\nu}) \tag{7}$$

from which we see that the axial response will always take the form of a sectioning response due to the second term of Eq. (7) together with a constant offset (McCabe *et al.*, 1996; Fewer *et al.*, 1997; Liang *et al.*, 1997). The designers of tandem scanning microscopes space their pinholes sufficiently far apart that the second term tends to dominate the first (c_0). However, this is at the expense of light budget. Since we cannot design a mask which sets $c_0 = 0$ because this represents the average value of $Q(t)$, which must be positive, we elect not to try to make the sectioning term dominate in Eq. (7) but rather to

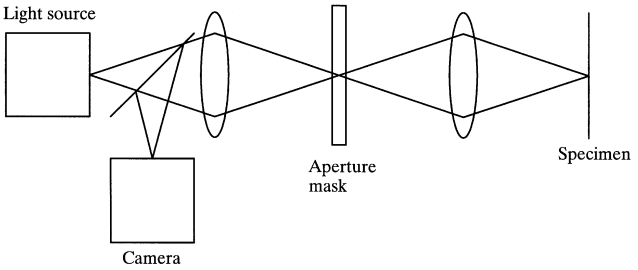

Fig. 2. Schematic diagram of the microscope system.

recognize that our system will inevitably produce a composite image which is a superposition of a wide-field image together with a sectioning image. Our approach will be to obtain both a composite and a wide-field image from which the sectioned image may be obtained by subtraction. In this sense our system configuration will be similar to that employed in our correlation microscope (Juškaitis *et al.*, 1996; Wilson *et al.*, 1996).

If we elect to use the simplest possible mask consisting of a single spatial frequency $\tilde{\nu}$ then the optical sectioning axial response, $I_s(u)$, given by the second term of Eq. (7), is

$$I_s(u) \sim f(\tilde{\nu})2\frac{J_1\left[2u\tilde{\nu}\left(1 - \frac{\tilde{\nu}}{2}\right)\right]}{2u\tilde{\nu}\left(1 - \frac{\tilde{\nu}}{2}\right)} \tag{8}$$

which of course depends on the value of $\tilde{\nu}$ chosen. We see that the maximum sectioning strength corresponds to $\tilde{\nu} = 1$. However, the light budget is reduced at high values of $\tilde{\nu}$ by a factor $f(\tilde{\nu})$.

In order to demonstrate the imaging capabilities of this kind of microscope we built the system of Fig. 2. The geometry is identical to that of a tandem scanning

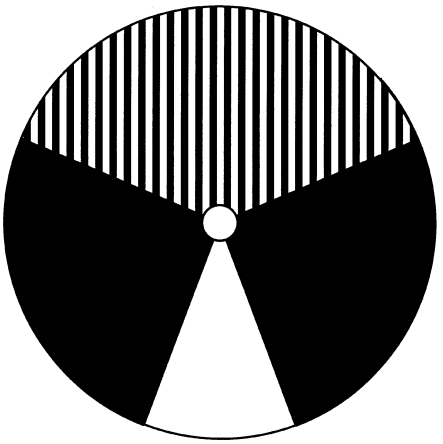

Fig. 3. Schematic diagram of the aperture mask showing the orientation of the grid lines.

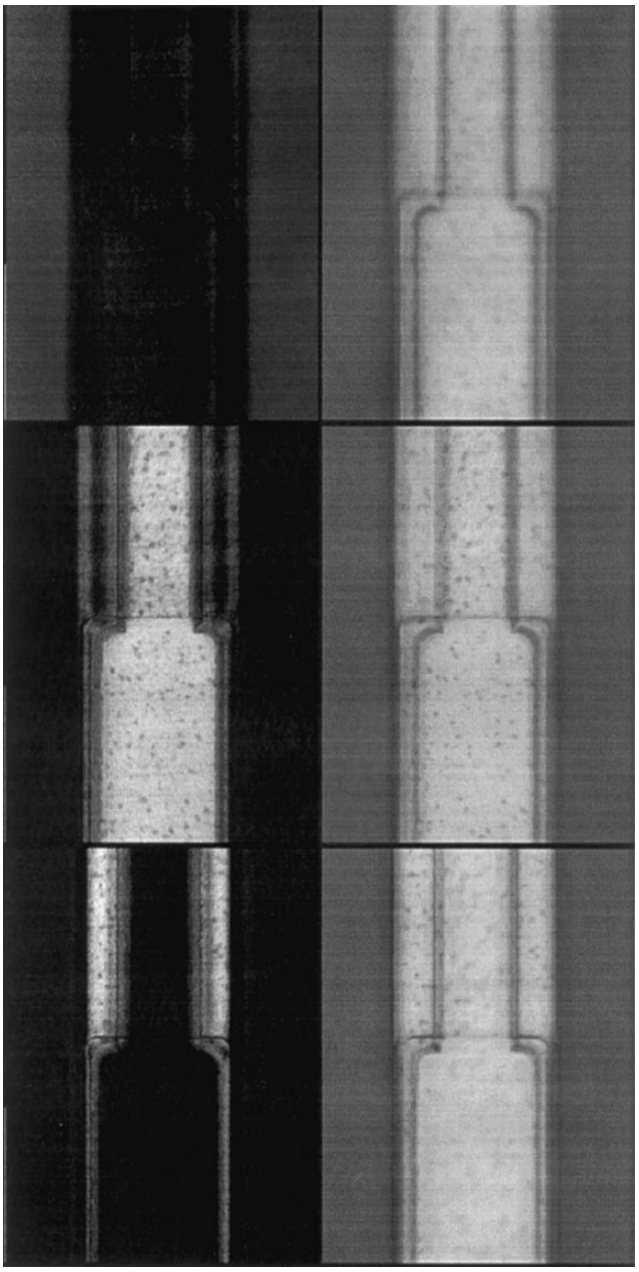

Fig. 4. A through-focus series of a portion of a semiconductor wafer. The left-hand column represent the optically sectioned images whereas the right-hand column shows the corresponding confocal images. The images were taken at focal settings 0·8 μm apart using a 100×, 0·95-NA Olympus MPlanApo objective lens. The image size is 43 μm × 57 μm.

microscope with the Nipkow disc replaced by an aperture mask. We produced the mask photolithographically by defining 80 μm lines on a 160 μm pitch in aluminium on a Perspex disc (Fig. 3). The transmittance was either zero or unity and the lines were orientated such that when the disc was rotated they essentially caused the one-dimensional grid to scan and rotate across the object. This orientation of the grid lines has the advantage of minimizing the slight asymmetry in the imaging which could have been produced by scanning a one-dimensional grid in one direction only across the object. Since it is necessary to subtract a conventional image from the composite image to obtain the optically sectioned image we also provided a blank sector on the disc to produce the conventional image. The system consisted of a standard 50-W lamp together with a narrow-band green filter ($\lambda = 546$ nm, $\Delta\lambda = 10$ nm). A simple CCD camera was used to capture both the composite and the conventional images. Our image capture system consisted of a PC together with a Matrox meteor imaging board which permitted us to perform real-time subtraction of the composite and wide-field images and so display the optically sectioned image and the conventional image simultaneously at TV rate.

Figure 4 shows a through-focus series of a portion of a semiconductor wafer. The images were obtained using a 100×0·95-NA Olympus MPlanApo objective lens and the images were taken at focal settings 0·8 μm apart. The left-hand column shows the optically sectioned images and the right-hand column the conventional image. The sectioning capabilities of our system are clearly visible.

The system is equally applicable to other imaging modes and, as an example, we show a Nomarski image in Fig. 5 of a series of 5-μm phase islands on a semiconductor wafer test pattern. The edges and general topography are well resolved.

We have presented a simple method of obtaining typically sectioned images of good quality and light efficiency by using a grid pattern rather than an array of widely spaced pinholes on a rotating disc. Our approach produces a composite image from which a wide-field image must be subtracted to reveal the optically sectioned image. The use of a one-dimensional grid pattern inevitably results in an asymmetry in the image formation. However, in practice in our configuration the differences are slight and we have obtained images which are similar in substance to pure confocal ones for a wide variety of specimens.

Acknowledgment

The work was funded by the Paul Instrument Fund of the Royal Society.

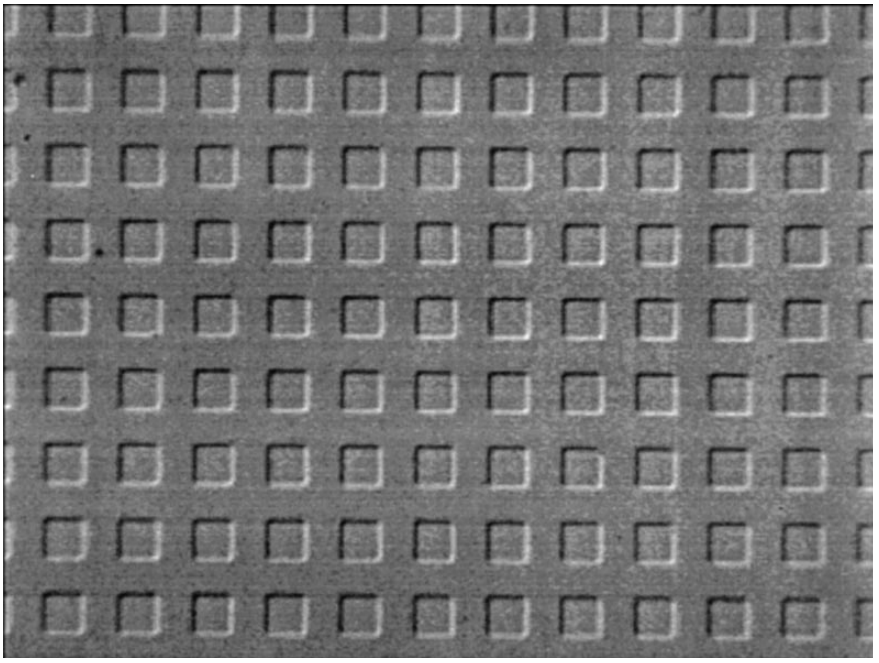

Fig. 5. A Normarski differential interference contrast image of 5-μm share phase islands within a semiconductor test pattern. The images were taken with a 50×, 0·7-NA Olympus Neo SPlan objective lens and the image size is 115 μm × 86 μm.

References

Egger, M.D. & Petráň, M. (1967) New reflected light microscope for viewing unstained brain and ganglion cells. *Science*, **157,** 305–307.

Fewer, D.T., Hewlett, S.J., McCabe, E.M. & Hegarty, J. (1997) Direct-view microscopy: experimental investigation of the dependence of the optical sectioning characteristics on pinhole-array configuration. *J. Microsc.* **187,** 54–61.

Juškaitis, R., Wilson, T., Neil, M.A.A. & Kozubek, M. (1996) Efficient real-time confocal microscopy with white light sources. *Nature*, **383,** 804–806.

Liang, M., Stehr, R.L. & Krause, A.W. (1997) Confocal pattern period in multiple-aperture confocal imaging systems with coherent illumination. *Opt. Lett.* **22,** 751–753.

McCabe, E.M., Fewer, D.T., Ottewill, A.C., Hewlett, S.J. & Hegarty, J. (1996) Direct-view microscopy in optical sectioning strength for finite-sized, multiple pinhole arrays. *J. Microsc.* **184,** 95–105.

Stockseth, P.A. (1969) Properties of a defocussed optical system. *J. Opt. Soc. Am.* **59,** 1314–1321.

Wilson, T. & Sheppard, C.J.R. (1984) *Theory and Practice of Scanning Optical Microscopy.* Academic Press, London.

Wilson, T. (ed.) (1990) *Confocal Microscopy.* Academic Press, London.

Wilson, T. & Hewlett, S.J. (1991) Optical sectioning strength of the direct-view microscope employing finite-sized pinhole arrays. *J. Microsc.* **163,** 131–150.

Wilson, T., Juškaitis, R., Neil, M.A.A. & Kozubek, M. (1996) Confocal microscopy by aperture correlation. *Opt. Lett.* **21,** 1879–1881.

Xiao, G.Q., Corle, T.R. & Kino, G.S. (1988) Real-time confocal scanning optical microscope. *Appl. Phys. Lett.* **53,** 716–718.